Research Square

Preprints are preliminary reports that have not undergone peer review.
They should not be considered conclusive, used to inform clinical practice,
or referenced by the media as validated information.

Dynamic Pulsed Magnetic Field Treatment Alters Germination Physiology, Transcriptomic Profiles, and Phytohormone Dynamics in Hulless Barley and Is Associated with Increased Grain Yield

Hong Wang
Qinghai University
Xijuan Yang
2007990025@qhu.edu.cn
Qinghai University
Yu Lin
Qinghai Miche Agricultural and Animal Husbandry Technology Co., Ltd
Ping Ma
Qinghai Tianyoude Technology Investment Management Group Co., Ltd

Research Article

Keywords: Hulless barley, Magnetic field treatment, Seed germination, Transcriptome, Hormone signaling, Agronomic yield

Posted Date: November 16th, 2026

DOI: https://doi.org/10.21203/rs.3.rs-11526884/v1

License: This work is licensed under a Creative Commons Attribution 4.0 International License.
Read Full License

Additional Declarations: No competing interests reported.

Dynamic Pulsed Magnetic Field Treatment Alters Germination Physiology, Transcriptomic Profiles, and Phytohormone Dynamics in Hulless Barley and Is Associated with Increased Grain Yield

Hong Wang[a,b,c]; Xijuan Yang[a,b,c]*; Yu Lin[d]; Ping Ma[e]

[a]*Academy of Agriculture and Forestry Sciences, Qinghai University, Xining 810016, China*

[b]*Key Laboratory of Qinghai Province Tibetan Plateau Agric-Product Processing, Qinghai University, Xining 810000, China*

[c]*Laboratory for Research and Utilization of Qinghai Tibet Plateau Germplasm Resources, Qinghai University, Xining 810016, China*

[d]*Qinghai Miche Agricultural and Animal Husbandry Technology Co., Ltd., Xining, Qinghai, China*

[e]*Qinghai Tianyoude Technology Investment Management Group Co., Ltd., Xining, Qinghai 810016, China*

**Corresponding author: E-mail:* 2007990025@qhu.edu.cn *(XJ Yang)*

Abstract: Dynamic pulsed magnetic-field seed priming represents a non-invasive physical approach associated with modifications in seed physiology and crop performance, yet its multi-layered effects remain poorly characterized in plateau-adapted hulless barley. Hulless barley (cv. Kunlun 14) seeds were assigned to a magnetic field treatment group (CH) and a non-magnetized control group (CK). CH seeds received a four-stage dynamic pulsed magnetic field (50–150 mT, 17 min total), and both groups were compared for germination phenotypes, physio-biochemical traits, time-course transcriptomes, 54 targeted phytohormones (47 retained after QC), and field grain yield. Magnetic priming was accompanied by enhanced germination starting from 24 h (17.80 % for CH vs. 14.53 % for CK, +22.5% at 24 h and +12.9%

at 48 h), accelerated radicle emergence (+43.6 % at 24 h), and increased bud length, root length, and seed-vigor index (+15.7 %). Physiologically, H_2O_2 accumulated in CH during early imbibition (+24.0% at 12 h, +18.7% at 24 h), ATP rose by 13.8% at 24 h, and α-amylase activity increased by 30.7% at 48 h. Antioxidant enzyme activities rose by 20.3–46.0%, while MDA decreased by up to 26.0%. Transcriptome analysis identified 7414 DEGs at 12 h, with starch and sucrose metabolism the most enriched pathway (fold = 15.27), and phytohormone profiling showed coordinated changes in auxin-, gibberellin-, cytokinin-, and brassinosteroid-associated hormones and genes, alongside altered ABA-related signaling. Field trials showed that magnetic treatment increased emergence, effective panicles, and grains per spike, raising yield by 6.81% in 2025 ($P < 0.01$) and 5.35% in 2026 ($P < 0.05$), for a combined increase of 6.10% across the two seasons, despite a small but significant reduction in 1000-grain weight. Our multi-omics dataset documents physiological, transcriptomic and hormonal changes correlated with magnetic-field priming and improved field-level yield performance in hulless barley. Note that these observations represent correlative responses; candidate magneto-perception modules inferred from transcriptome data require further genetic-functional validation.

Keywords: Hulless barley; Magnetic field treatment; Seed germination; Transcriptome; Hormone signaling; Agronomic yield

1. Background

Hulless barley (*Hordeum vulgare var. coeleste L.*), a hulless naked barley

endemic to the Qinghai–Tibet Plateau, has become a staple crop in the high-altitude areas of the region owing to its strong drought- and cold-tolerance and short growing period [1]. However, the alpine environment often leads to low germination rates and unstable yields, severely restricting quality improvement and yield stability [2]. Because seed germination and early seedling establishment directly determine subsequent growth and final yield, essential for enhancing the industrial value of hulless barley. Therefore, developing an effective seed treatment is critical for hulless barley production.

The Qinghai–Tibet Plateau is an ecologically fragile region, and environmental sustainability is an important consideration in agricultural practices. Chemical inputs, however, raise residue and ecological concerns [3, 4]. Magnetic field treatment, by contrast, is a non-invasive, residue-free, and efficient physical priming strategy that improves seed germination, seedling growth, yield and quality, as well as stress tolerance across horticultural and agricultural crops [5-7]. Previous studies have shown that magnetic treatment has raised germination percentage and seedling vigor in sunflower (50 mT, 45 min) and maize (200 mT, 30 s), and improved germination rate, vigor index, and dry matter accumulation in soybean (50-100 mT) [8-10]. Field trials indicate that these early responses can translate into grain yield gains: pre-sowing magnetic treatment at 60 and 40 mT increased wheat grain yield by 18.0% and 23.8% at two sites, respectively, through increases in spike number and grains per spike [11]. However, in plateau environments, the application of magnetic field treatment to hulless barley for improving germination vigor and related traits has not

been reported.

Although magnetic treatment has been shown to activate antioxidant enzymes and reduce oxidative damage [12, 13], alter hormone balance [14], and potentially act via cryptochrome-mediated radical pair mechanisms regulating auxin and gibberellin signaling [15-18], these mechanisms are largely inferred from other crops. In wheat, magnetic field treatment induces *TaHY5* expression, inhibits jasmonate biosynthesis, and promotes nitrogen assimilation [19]. These studies, however, have been restricted mainly to a single physiological layer or a single time point; how antioxidant defense, carbon-energy metabolism, and hormone signaling are coordinated during germination, and which transcriptional networks link them, remain uncharacterized. In hulless barley in particular, neither the stage-specific transcriptional response to magnetic treatment nor its association with field establishment and grain yield has been examined. Therefore, integrated transcriptomic, hormonal, and physio-biochemical analyses were performed to elucidate the mechanisms by which magnetic field treatment improves hulless barley germination and yield.

We hypothesized that magnetic priming is accompanied by temporal reprogramming of antioxidant defense, carbon-energy metabolism and growth-promoting hormone signaling, which may contribute to enhanced germination and field yield of hulless barley, alongside stage-specific transcriptional reprogramming. To test this hypothesis, seeds (cv. Kunlun 14) were sampled at 0, 12, 24, 48, and 72 h under magnetized and non-magnetized treatments, and integrated transcriptome, phytohormone, and physio-biochemical analyses were performed. This

study had four objectives: to quantify treatment-associated changes in germination and seedling traits; to characterize physiological and transcriptional responses during early imbibition; to examine changes in phytohormone profiles and their associations with gene expression; and to evaluate whether early treatment-associated responses were accompanied by differences in field establishment and grain yield.

2. Methods

2.1 Plant Materials and Germination Conditions

The hulless barley cultivar “Kunlun 14” was used as the experimental material. Plump, uniformly sized seeds free of pests and disease lesions were selected, and seed moisture content was measured in triplicate before treatment. The mean moisture content was 12.15 ± 0.30% (mean ± SD, n = 3), and all seeds were standardized to this uniform moisture content prior to magnetic field treatment.

Dry seeds designated for magnetic field treatment (CH) were loaded into a custom-built closed electromagnetic chamber jointly developed by the School of Automation, South China University of Technology, and Guangdong Miche Network Technology Co., Ltd. The treatment was performed using a programmable pulsed magnetic field device with a four-stage dynamic magnetization program. The program was set as follows: stage 1, 50 mT pulsed magnetic field at 10 Hz with 50% duty cycle for 2 min; stage 2, 100 mT pulsed magnetic field at 16 Hz with 50% duty cycle for 5 min; stage 3, 150 mT pulsed magnetic field at 20 Hz with 50% duty cycle for 8 min; stage 4, 50 mT static magnetic field for 2 min. Magnetic field treatment

parameters were generated using a pre-trained deep learning model as described in Chinese Invention Patent Application Publication No. CN121256250A. Hyperspectral data were acquired in the 400-1000 nm range, including reflectance and transmittance spectra, and were preprocessed by noise removal, normalization, and feature extraction. The model was trained with seed germination rate and growth activity as outputs, and generated magnetic field frequency, waveform, direction, duration, and field intensity. The electromagnetic field generation device consisted of parallel-plate electrodes and Helmholtz coils, with real-time monitoring and feedback control. A 50% duty cycle indicates that the magnetic field was switched on and off for equal durations within each pulse cycle. The total treatment duration was 17 min. The chamber temperature was maintained at 25 ± 1 ℃ throughout the treatment. The electromagnetic field generation device (comprising parallel-plate electrodes and Helmholtz coils) operated within a closed chamber with real-time monitoring and feedback control to ensure treatment consistency.

The control group (CK) consisted of the same seed batch and underwent identical sterilization, soaking, and incubation protocols without magnetic field exposure. Briefly, seeds from both groups were surface-sterilized in 0.1% $HgCl_2$ solution for 10 min, rinsed 3-5 times with sterile distilled water, and then soaked. Sterilized seeds were evenly distributed in 20 cm-diameter Petri dishes lined with two layers of sterile filter paper, with 500 seeds per dish. All samples were incubated at 24 ± 1 °C under a 16 h light / 8 h dark photoperiod. A thin layer (~2 mm) of sterile water was maintained in each dish, and additional sterile water was supplied regularly to

maintain suitable moisture for seed germination. Three biological replicates were performed for each treatment.

2.2 Field Experiment Site, Design, and Crop Management

The field experiment was conducted over two consecutive growing seasons (2025 and 2026) at the Germplasm Resource Innovation Experimental Base of Qinghai University, Xining, Qinghai Province (36°37′N, 101°45′E, elevation 2309 m). The growing seasons spanned from April 13 to July 23, 2025, and April 9 to July 22, 2026. The soil is classified as chestnut soil. Pre-sowing topsoil (0–20 cm) properties in 2025 and 2026 were as follows: pH 8.35 and 8.44, organic matter 17.0 and 16.6 g kg^{-1}, alkali-hydrolyzable N 62.5 and 63.9 mg kg^{-1}, available P 18.3 and 30.5 mg kg^{-1}, available K 145.0 and 147.0 mg kg^{-1}, total N 1.07 and 1.18 g kg^{-1}, total P_2O_5 2.47 and 2.60 g kg^{-1}, and total K_2O 25.4 and 24.5 g kg^{-1}, respectively. These values indicate a consistent, slightly alkaline basal soil fertility across the two years.

The experiment used a randomized block design with two treatments (magnetic field treatment, CH; untreated control, CK) and three replications. Plot sizes were 10.8 m^2 (5.4 m × 2.0 m, 10 rows) in 2025 and 30 m^2 (5.0 m × 6.0 m, 30 rows) in 2026, with a uniform row spacing of 0.20 m. The sowing rate was 315 kg ha^{-1} in both years, and field management followed local conventional practices. Basal fertilization was applied identically across years, consisting of 56.25 kg ha^{-1} urea (46% N) and 112.5 kg ha^{-1} diammonium phosphate (18% N, 46% P_2O_5), totaling 46.13 kg N ha^{-1} and 51.75 kg P_2O_5 ha^{-1} (equivalent to 22.56 kg P ha^{-1}). No potassium fertilizer was applied.

158 **2.3 Sample Collection**

159 Samples were collected at 0 h (seeds before imbibition) and at 12, 24, 48, and 72
160 h of germination, with three biological replicates per time point. All samples (whole
161 seeds or young buds) were placed into cryovials, rapidly frozen in liquid nitrogen, and
162 stored at −80 °C for subsequent determination of physio-biochemical indicators, RNA
163 extraction, and hormone analysis.

164 For germination phenotype analysis, with 500 seeds as the counting unit,
165 germination rate and root formation rate were recorded at each time point. At 24-h
166 intervals, 30 germinated seedlings were randomly selected to measure bud length,
167 root length, bud fresh weight, and root fresh weight. Germination energy was
168 measured at 72 h, while root: shoot ratio, relative water content, stored substance
169 translocation rate, germination index, and vigor index were measured at 168 h. All
170 indicators were measured with three biological replicates.

171 Samples from the magnetic field treatment group at different germination time
172 points were denoted as H0, H12, H24, H48, and H72, while samples from the
173 non-magnetized control group were denoted as K0, K12, K24, K48, and K72.
174 Hereafter, the magnetic field treatment group is abbreviated as CH and the control
175 group as CK; the original labels K0–K72 correspond to CK0–CK72, and H0–H72
176 correspond to CH0–CH72.

177 **2.4 Physio-Biochemical Indicator Determination**

178 The activities of superoxide dismutase (SOD, EC 1.15.1.1), peroxidase (POD,
179 EC 1.11.1.7), catalase (CAT, EC 1.11.1.6), and glutathione peroxidase (GPx, EC

1.11.1.9), as well as malondialdehyde (MDA) content, were determined using corresponding assay kits from Beijing Solarbio Science & Technology Co., Ltd. (Solarbio). α-Amylase (EC 3.2.1.1) activity and ATP and H_2O_2 contents were determined using kits from Boxbio. Soluble sugar, soluble protein, and free proline contents were measured according to the methods of [20]. All measurements were performed with three biological replicates using a microplate reader (Multiskan SkyHigh, Thermo Scientific, USA) or a UV–Vis spectrophotometer (TU-1810PC, Beijing Purkinje General Instrument Co., Ltd., China).

2.5 RNA Extraction and Detection

Total RNA was extracted and used for strand-specific library construction. Libraries were sequenced by Metware Biotechnology Co., Ltd. (Wuhan, China) on the MGI sequencing platform. After quality filtering with fastp, clean reads were aligned to the MorexV3 reference genome using HISAT2. Gene-level counts were obtained with featureCounts, and FPKM values were calculated for expression visualization. Differentially expressed genes were identified using DESeq2 based on raw integer read counts, with $|\log2FC| \geq 1$ and $FDR < 0.05$.

2.6 qRT-PCR Verification

To verify the reliability of transcriptome sequencing results, five key genes in hormone signaling pathways were randomly selected for qRT-PCR verification. Total RNA was extracted using the TaKaRa MiniBEST Plant RNA Extraction Kit (Code No. 9769), and 1 μg RNA was reverse-transcribed into cDNA using PrimeScript™ RT reagent Kit with gDNA Eraser (TaKaRa, RR047A). With diluted cDNA as the

template, qRT-PCR was performed on a LightCycler 4800 (Roche) real-time PCR instrument with TB Green® Premix Ex Taq™ II (TaKaRa, RR820A). The reaction volume was 20 μL, with three technical replicates per sample. Primers for target genes and the reference gene (18S rRNA) were synthesized by Sangon Biotech (Shanghai) Co., Ltd.; primer sequences are listed in Table S1. The reaction program was as follows: pre-denaturation at 95 °C for 30 s, followed by 40 cycles of denaturation at 95 °C for 5 s and annealing at 60 °C for 30 s. The melting curve was generated according to the default program of the instrument. Relative expression levels of target genes were calculated using the $2^{-\Delta\Delta Ct}$ method.

2.7 Phytohormone Determination

Targeted phytohormone profiling was performed by Shanghai BIOTREE Biological Technology Co., Ltd. (Shanghai, China). A total of 54 target compounds were quantified. After filtering metabolites with >50% missing values and imputing remaining missing values, 47 compounds passed quality control and were used for downstream analysis. Data were log-transformed and centered, and principal component analysis (PCA) was performed using SIMCA 18.0.1 (Sartorius Stedim Data Analytics AB, Umea, Sweden). Univariate ANOVA, hierarchical clustering, KEGG annotation, and pathway analysis were conducted against the Hordeum vulgare database.

2.8 Data Analysis

After filtering with fastp, raw transcriptome data were aligned to the reference genome using HISAT2, and transcripts were assembled using StringTie.

FeatureCounts was used to generate read counts, and FPKM values were calculated accordingly, while DESeq2 was used to screen differentially expressed genes with adjusted $P < 0.05$ and $|\log_2FC| \geq 1$. GO and KEGG enrichment analyses were then performed. For phytohormone data, indicators with a missing value proportion exceeding 50% were removed, and the remaining missing values were imputed. ANOVA, t-tests, and PCA were comprehensively used for statistical analysis. R was used for Z-score normalization and visualization. Physio-biochemical indicators were compiled in Excel and statistically analyzed using SPSS 23.0, and charts were plotted using Origin 2021 and the lims2 platform (https://lims2.com/). The field experiment was arranged in a randomized complete block design with three replications per treatment per year. Within each year, CK and CH plots were paired within the same block, and plot means were used as the statistical unit. Grain yield was converted to $kg \cdot ha^{-1}$ using the net plot area (10.8 m^2 in 2025 and 30 m^2 in 2026). For field data, two-way analysis of variance (ANOVA) was performed using SPSS 26.0, with year (2025, 2026) and treatment (CK, CH) as fixed factors, including the year × treatment interaction. Within each year, CK and CH were compared using independent-sample t-tests. Data are presented as mean ± standard deviation (SD) (n = 3 plots). Significance was set at $P < 0.05$. Different lowercase letters in the tables indicate significant differences between CH and CK within the same year ($P < 0.05$). The combined increase across the two seasons was calculated as the arithmetic mean of the two seasonal percentage increases.

3. Results

3.1 Pre-sowing magnetic treatment promotes germination and early seedling growth

Pre-sowing magnetic treatment advanced germination and increased seedling growth relative to non-magnetized controls (Fig. 1A–1F). Germination rate in CH exceeded that of CK from 24 h onward, and the difference declined progressively thereafter (24 h, +22.5%, $P < 0.05$; 48 h, +12.9%, $P < 0.01$; 72 h, +6.3%, $P < 0.05$); by 168 h, germination rates reached 96.60% and 94.07% in CH and CK, respectively. Root formation showed a stronger response than germination. At 24 h, the root formation rate of CH was 16.47%, 43.6% higher than that of CK ($P < 0.01$), and the advantage was sustained through 48 h (+9.4%, $P < 0.01$). These results indicate that magnetic treatment accelerated both germination onset and root formation during imbibition.

Four organ traits were measured to characterize growth responses: bud weight, bud length, root number, and root length (Fig. 1A–1D). The CH–CK differences for all four traits were largest during 72–96 h, although the magnitude of response varied among traits. Bud weight was 11.5%–12.1% higher in CH between 72 and 120 h ($P < 0.01$), but the difference narrowed to 4.0%–6.1% at 144–168 h, losing significance by 168 h ($P > 0.05$). Bud length was 13.6%–46.1% higher in CH between 72 and 144 h ($P < 0.05$ to $P < 0.01$) and remained 8.0% longer at 168 h (CH, 9.61 cm; CK, 8.90 cm; $P < 0.01$). Root number was 6.7%–11.3% higher in CH between 72 and 120 h ($P < 0.05$ to $P < 0.01$). Root length showed the largest response of the four traits, peaking

at 96 h (+57.2%, P < 0.001) and remaining 46.7% and 27.4% higher at 72 h (P < 0.001) and 120 h (P < 0.01), respectively. Magnetic treatment therefore acted most strongly on root elongation among the organ traits measured.

Vigor indices were consistent with the morphological responses (Fig. 1G). Germination energy was 6.3% higher in CH than in CK (92.87% vs. 87.40%, P < 0.05), and the vigor index increased from 729.86 in CK to 844.29 in CH, an increase of 15.7%. The stored substance transport rate was also higher in CH (0.69 vs. 0.63, P < 0.01), whereas root–shoot ratio and relative water content did not differ between treatments. Representative phenotypes are shown in Fig. 1H. The germination advantage was most pronounced during the first 72 h and stabilized thereafter. Samples were collected at 0, 12, 24, 48, and 72 h, and the early seedling growth phase (from 72 h onward), and were subjected to physio-biochemical, transcriptomic, and phytohormone analyses.

3.2 Pre-sowing magnetic treatment enhances antioxidant defense and shifts carbon metabolism toward energy utilization

Antioxidant system- and energy metabolism-related indicators were measured to examine the physiological basis of the growth advantage described above (Fig. 2A–2K). Antioxidant enzyme activities were generally higher in CH than in CK (Fig. 2A–2E). CAT activity was 46.0% higher in CH at 12 h (P < 0.05) and 34.9% higher at 72 h (129.02 vs. 95.66 $U \cdot g^{-1}$, P < 0.01), and GPx activity was 7.1% higher at 72 h (P < 0.05). SOD and POD activities followed similar temporal patterns, both peaking at 48 h and remaining higher in CH at 72 h; SOD activity was 41.3% and 39.9% higher at

48 and 72 h, respectively ($P < 0.01$), and POD activity was 45.5% and 20.3% higher over the same intervals ($P < 0.01$). Enzyme activities increased with germination time in both treatments, most rapidly between 12 and 48 h, with a larger increase in CH. MDA content in CH was lower than in CK from 24 to 72 h, declining by 26.0%, 17.7%, and 9.3%, respectively ($P < 0.01$). H_2O_2 content was slightly higher in CH at 0 h (+6.7%, $P > 0.05$) and significantly higher at 12 and 24 h (+24.0%, $P < 0.01$; +18.7%, $P < 0.05$, respectively), but did not differ at 48 or 72 h. The transient increase in H_2O_2 was followed by enhanced enzymatic defense and a sustained reduction in MDA, indicating that redox-balance shifts and reduced oxidative damage were observed under magnetic priming during germination.

Magnetic treatment also altered energy metabolism and the mobilization of stored substances (Fig. 2G–2K). α-Amylase activity in CH was 7.6% higher than in CK at 12 h ($P < 0.01$) and 30.7% higher at 48 h ($P < 0.01$), indicating that starch degradation was activated from early imbibition. Soluble sugar content in CH was correspondingly 4.4% lower at 24 h (Fig. 2I), while ATP content was 13.8% higher at 24 h ($P < 0.05$) (Fig. 2H); the concurrent decrease in soluble sugar and increase in ATP indicates that stored carbon was directed toward energy metabolism rather than accumulating as soluble sugar. Soluble protein content was 24.9% higher in CH than in CK at 48 h (4.72 vs. 3.78 $mg \cdot g^{-1}$) but 12.7% lower at 72 h (Fig. 2J). Free proline content was 26.5% and 12.0% lower in CH at 24 and 48 h, respectively ($P < 0.01$), and converged with CK by 72 h (Fig. 2K). These patterns indicate transient changes in protein metabolism and reduced osmotic stress during early germination, consistent

with previous observations [21]. The antioxidant and carbon metabolism responses were both most pronounced around 24 h, suggesting that oxidative signaling and starch-to-energy conversion acted concurrently during imbibition. These physiological changes indicate that magnetic treatment may induce broader transcriptional reprogramming; time-course transcriptome analysis was therefore performed.

3.3 Magnetic field treatment induces transcriptome reprogramming during hulless barley germination

3.3.1 Transcriptome sequencing quality and identification of differentially expressed genes

Given the significant physiological changes induced by magnetic field treatment, we hypothesized that it might exert a global regulatory effect on gene transcription; therefore, transcriptome sequencing was performed. A total of 224.60 Gb of high-quality Clean Data were obtained, with Q30 percentages of all samples not less than 96.75% and GC content ranging from 52.01% to 53.91%, indicating reliable sequencing quality (Supplementary Table S2: Quality statistics of sequencing reads).

Gene expression levels were quantified using the FPKM method. Although germination stage was the primary source of transcriptome variation, CH and CK were clearly separated at each time point, indicating that magnetic priming produced specific expression changes superimposed upon the intrinsic developmental program (Fig. 3A).

Differentially expressed gene (DEG) screening was performed using the criteria $|\log_2 FC| \geq 1$ and FDR < 0.05. In the five comparison groups, H0 vs. K0, H12 vs. K12, H24 vs. K24, H48 vs. K48, and H72 vs. K72, 130, 7,414, 1,168, 2,278, and 898 DEGs were identified, respectively (Fig. 3C). The largest number of DEGs was detected at 12 h, indicating that 12 h represented the period with the most prominent transcriptional differences between magnet-primed and control seeds. No DEGs were shared among the five comparison groups (Fig. 3B), suggesting that the gene expression responses induced by magnetic field treatment were highly time-specific. Given the pronounced transcriptomic differences, we next examined stage-specific functional enrichment of DEGs.

3.3.2 Magnetic field treatment induces stage-specific functional enrichment of differentially expressed genes

DEGs induced by magnetic treatment showed distinct stage-specific functional enrichment patterns across germination time points (Fig. S1-S2). Unless otherwise stated, all DEGs described below refer to CH vs CK comparisons at each time point. At 0 h, magnetic treatment-induced DEGs were enriched in membrane remodeling (GO:0016134, GO:0016137) and water homeostasis (GO:0009992), together with glycosphingolipid and selenocompound metabolism (KEGG), suggesting that magnetic treatment was associated with osmotic regulation upon imbibition.

At 12 h, 7414 DEGs (3 945 up-regulated and 3 469 down-regulated) reflected pronounced transcriptional differences under magnetic priming. GO terms related to nucleosome assembly (GO:0006334), mitotic cell cycle (GO:1903047), and

translation (GO:0006412) were significantly up-regulated, along with widespread activation of Cyclin/CDK and RPS/RPL family genes. Starch and sucrose metabolism emerged as the core enriched KEGG pathway (enrichment fold = 15.27), accompanied by alanine/aspartate/glutamate metabolism and purine metabolism. These results show enrichment of cell-proliferation and energy-metabolism-related gene sets in CH samples during the transition from dormancy to germination. The strong enrichment of starch and sucrose metabolism at 12 h is highly consistent with the enhanced α-amylase gene expression previously reported in magnetically treated brown rice [22].

At 24 h, magnetic treatment-induced DEGs were enriched in chloroplast structural assembly (GO:0009658), photosynthetic pigment synthesis (GO:0015995), and ROS scavenging (GO:0019203). The Photosynthesis-antenna proteins pathway was significantly enriched for the first time (enrichment factor = 18.72), together with phenylpropanoid biosynthesis and diterpenoid biosynthesis, marking the onset of autotrophic system assembly. Similar early activation of photosynthetic and antioxidant pathways has been observed in magnetically treated soybean [23] and Arabidopsis [24].

At 48 h, among magnetic treatment-induced DEGs, down-regulated genes began to predominate (1459 down vs. 819 up). Organ development-related genes (ARF/Aux/IAA and WOX families; GO:0030154, GO:0048366) showed altered expression, while stress response genes (HSP family; GO:0009408) were significantly down-regulated. The Photosynthesis-light reactions pathway (enrichment factor =

21.35) and auxin-mediated signaling were simultaneously enriched, suggesting coordinated regulation of growth and defense.

At 72 h (898 DEGs), meristem maintenance (GO:0009950) and phase transitions (GO:0009965) enriched, while phenylpropanoid metabolism declined. Carbon fixation showed the highest enrichment (24.68), and organ development pathways appeared, indicating a shift from vegetative growth to differentiation. Overall, these stage-specific changes were closely synchronized with the physiological progression of seed germination. These stage-specific enrichments suggest temporal coordination of multiple pathways by magnetic treatment. We next examined hormone signaling networks, which are central to the regulation of seed germination.

3.3.3 Magnetic field treatment reshapes hormone signaling networks during germination

To reveal how magnetic treatment regulates germination, eight hormone signaling pathways were integrated into a regulatory network (Fig. 4). Heatmaps showed gene expression differences between CH and CK at each time point.

Growth-promoting pathways were coordinately activated. Auxin precursors 3-IAN and IA were elevated at 0 h, while free IAA transiently declined at 12 h. The auxin influx carrier gene was up-regulated 3.8-fold in CH relative to CK at 12 h ($P < 0.05$), and this was accompanied by up-regulation of Aux/IAA early response genes, including HORVU.MOREX.r3.5HG0509760 (2.8-fold higher in CH than in CK at 12 h) and another family member (3.2-fold higher in CH than in CK at 12 h). Cytokinin and brassinosteroid pathways jointly promoted cell division: trans-zeatin was elevated

399 at 24 h, the ARR-A family gene HORVU.MOREX.r3.3HG0321410 was up-regulated
400 2.83-fold in CH relative to CK at 12 h, and BAK1 was up-regulated 3.2-fold in CH
401 relative to CK at 12 h. In the gibberellin pathway, DELLA
402 (HORVU.MOREX.r3.2HG0130900) was down-regulated by 67% in CH relative to
403 CK at 12 h, while GA_{20} and GA_7 accumulated from 0 to 24 h, indicating release of
404 gibberellin signaling inhibition.

405 ABA-related genes showed transcriptional changes. ABA content decreased at
406 12 h, while ACC increased. PP2C was down-regulated by 64%, and PYL and SRK2
407 were down-regulated by 74% in CH relative to CK at 12 h, collectively indicating
408 transcriptional changes in ABA-related signaling and in dormancy-related regulation.

409 JA/SA defense pathways showed a dynamic temporal pattern. JAZ and COI1
410 were down-regulated by 60% and 46% in CH relative to CK at 12 h, with decreased
411 JA content. At 48–72 h, JA partially recovered and MYC2 showed moderate
412 expression. NPR1 was down-regulated by 76% in CH relative to CK at 48 h, whereas
413 PR-1 genes were induced at 24 h. These results indicate that basal defense signaling
414 was reduced during early germination and then moderately activated after growth
415 stabilization, optimizing the allocation of growth and defense resources. This
416 temporal defense pattern differs from wheat, where magnetic treatment continuously
417 suppresses jasmonate biosynthesis through TaHY5 [19], suggesting that crop species
418 may adopt distinct defense strategies in response to magnetic treatment.

419 **3.3.4 Magnetic field treatment alters hormone metabolic profiles during**
420 **germination**

Differential hormones between CH and CK were identified at each time point (VIP > 1, $P < 0.05$; Fig. 5). The number of differential hormones showed a stage-specific pattern. At 0 h, 9 hormones were up-regulated and 3 down-regulated, indicating rapid hormone pathway activation upon imbibition. At 12 h, down-regulated hormones (11) outnumbered up-regulated ones (8) for the first time, coinciding with decreased ABA and down-regulated cytokinin transport forms. At 24 h, the hormone response peaked with 18 up-regulated hormones, led by trans-zeatin. At 48 h and 72 h, up- and down-regulated hormones tended to balance (14 up vs. 8 down at 48 h; 16 up vs. 14 down at 72 h), reflecting the transition toward metabolic homeostasis and differentiation.

During 0-12 h, auxin precursors and GA_{20}/GA_7 increased at 0 h, while cytokinin transport forms decreased. At 12 h, ABA decreased and ACC increased, marking dormancy release. Auxin conjugates increased, free IAA declined transiently, and trans-zeatin decreased, reflecting metabolic reorganization toward germination.

At 24 h, GA_{20}, GA_7, brassinolide, and free IAA rebounded and were elevated, promoting elongation before radicle emergence. Trans-zeatin was strongly up-regulated for cell division, while auxin conjugates remained high to buffer IAA and maintain homeostasis.

During 48-72 h, GA_{20}, IAA, and brassinolide remained elevated, while auxin conjugates declined. At 48 h, ABA rebounded and tryptamine increased, indicating stress preparation. By 72 h, IAA and auxin conjugates decreased, while 2-oxoindole-3-acetic acid increased, reflecting attenuated auxin signaling.

Trans-zeatin rose again to maintain meristem activity, while tryptamine remained high, suggesting normalized secondary metabolism.

These hormone metabolic patterns were consistent with the hormone signaling pathway gene expression (Fig. 4), providing metabolite-level evidence that magnetic treatment is associated with temporal changes in the hormone network, characterized by early dormancy release, mid-stage growth promotion, and late-stage differentiation guidance.

3.4 qRT-PCR validation of key hormone signaling genes regulated by magnetic field treatment

To verify RNA-seq reliability, five hormone signaling genes (IAA, ARR-A, DELLA, ABF, and NPR1) were selected for qRT-PCR across five germination time points. The expression trends of all five genes were consistent with the RNA-seq FPKM values (Supplementary Table S3, Fig. 6). IAA and ARR-A were up-regulated in CH at 12–24 h, whereas DELLA, ABF, and NPR1 were down-regulated at 12 h or 48 h, consistent with the transcriptome data. These results confirm the reliability of the RNA-seq profiles.

3.5 Integrated gene–hormone–physiology correlation analysis

After reliability verification of transcriptome and hormone data, multi-omics joint analysis was performed to explore associations among genes, hormones, and physiological indicators. Pearson correlations were calculated across all sampling time points. All correlation analyses in this section are exploratory and cannot establish causal relationships between variables. The results showed that magnetic

field treatment exerted precise regulatory effects on hormones and physiological indicators in hulless barley (Fig. 7A). The growth-promoting hormone Gibberellin A_{20} showed a strong positive correlation with trans-Zeatin, and both were significantly positively correlated with SOD activity, POD activity, ATP content, and α-amylase activity, forming a core growth-promoting regulatory module. In contrast, Abscisic acid was strongly negatively correlated with these physiological indicators, showing clear antagonism with Gibberellin A_{20}. The defense hormones salicylic acid and jasmonic acid were significantly positively correlated with each other and were closely associated with stress-resistance-related indicators such as free proline and POD activity. At the functional gene level, growth-promoting genes, including HORVU.MOREX.r3.5HG0509760 and HORVU.MOREX.r3.3HG0321410, showed very high positive correlations with each other, while defense-related genes, including HORVU.MOREX.r3.7HG0690270 and HORVU.MOREX.r3.7HG0713160, also exhibited strong positive correlations. These two gene categories formed specific associations with corresponding hormones and physiological indicators, reflecting distinct functional clustering of gene expression.

In the unmagnetized group, correlations were relatively weak (e.g., GA_{20}-SOD: r = 0.897; SA–JA: r = 0.633). After magnetic treatment, these were stronger (GA_{20}-SOD: r = 0.965; SA–JA: r = 0.878; JA–proline: r = 0.749) (Fig. 7B–7C). The negative correlation between Abscisic acid and α-amylase activity decreased from −0.939 to −0.801, suggesting alleviation of excessive inhibition on carbon metabolism. In addition, the sensitivity of defense genes to salicylic acid was

enhanced, and the functional differentiation between growth-promoting and defense gene clusters became more distinct, forming an efficient targeted regulatory network.

The grouped fitting scatter plots further confirmed the regulatory enhancement induced by magnetic field treatment (Fig. 7D–7G). In the magnetic field treatment group (CH), the goodness of fit for Gibberellin A_{20} versus SOD activity reached R^2 = 0.931, with a slope of 839, both higher than those in the control group (CK) (R^2 = 0.805, slope = 724). Abscisic acid showed a strong negative correlation with ATP, with R^2 = 0.833 and an absolute slope value of 46 in CH, higher than those in CK (R^2 = 0.798, slope = 36). NPR1 showed a strong positive correlation with salicylic acid in CH (R^2 = 0.775), whereas only a weak positive correlation was observed in CK (R^2 = 0.312). The R^2 for jasmonic acid versus proline increased from 0.388 in CK to 0.562 in CH. These correlations suggest that magnetic treatment may strengthen the coordination among gibberellin signaling, antioxidant defense, and energy metabolism, although causal relationships remain to be established.

3.6 Magnetic field treatment improves field establishment, grain yield, and yield components

Field performance and yield components were compared between CH and CK across the two growing seasons (Table 1). Magnetic treatment significantly increased field emergence in both years. In 2025, the 2–3 leaf emergence peak in CH was 684.67 ± 11.00 plants·m^{-2}, which was 8.56% higher than that of CK (630.67 ± 14.71 plants·m^{-2}, P<0.05). In 2026, CH emergence was 678.11 ± 9.01 plants·m^{-2} 4.63% higher than CK (648.11 ± 6.71 plants·m^{-2}, P<0.05). Two-way ANOVA showed a

highly significant treatment main effect for emergence (P<0.001) and a non-significant year × treatment interaction (P=0.089), indicating that the promotion of field establishment by magnetic treatment was consistent across the two years.

Effective panicles per unit area were significantly increased by magnetic treatment in both seasons: 382.78 ± 6.87 vs. 354.89 ± 11.08 panicles·m^{-2} in 2025 (+7.86%, P<0.05) and 376.55 ± 9.93 vs. 338.56 ± 12.41 panicles·m^{-2} in 2026 (+11.22%, P<0.05). The treatment main effect was highly significant (P<0.001), and the year × treatment interaction was not significant (P=0.419). However, no significant difference was detected in effective panicles per plant between treatments in either year (2025: 1.447 ± 0.068 vs. 1.377 ± 0.050; 2026: 1.303 ± 0.058 vs. 1.313 ± 0.051; P>0.05; treatment main effect P=0.391), indicating that the increased population panicles in CH were primarily attributed to improved seedling establishment and population density rather than excessive tillering per individual.

Grains per spike showed a significant treatment main effect (P=0.017), although the within-year differences did not reach significance (2025: 48.57 ± 0.67 vs. 47.04 ± 0.77; 2026: 47.95 ± 0.41 vs. 46.67 ± 1.18; P>0.05). A slight but significant reduction in 1000-grain weight was observed under magnetic treatment (treatment main effect P=0.027), with 2025 showing a significant decrease (46.38 ± 0.31 vs. 47.06 ± 0.28 g, P<0.05) and 2026 showing a non-significant decrease (46.17 ± 0.74 vs. 46.89 ± 0.27 g, P>0.05). Despite this, grain yield was significantly increased in both seasons. On a per hectare basis, CH produced 7061.10 ± 137.08 kg·ha^{-1} in 2025, 6.81% higher than CK (6611.10 ± 59.80 kg·ha^{-1}; P<0.01), and 6597.44 ± 91.35 kg·ha^{-1} in 2026, 5.35%

higher than CK (6262.44 ± 106.75 kg·ha^{-1}; P<0.05). The treatment main effect for grain yield was highly significant (P<0.001), and the year × treatment interaction was not significant (P=0.360).

These results indicate that magnetic field treatment was associated with improved field establishment and consistent grain yield gains in hulless barley. The yield advantage was mainly driven by increased effective panicles and grains per spike, which compensated for the slight reduction in 1000-grain weight, forming a "spike-number-dominant, grain-number-supplementary, and slightly reduced grain-weight" yield gain pathway.

4. Discussion

This study compared magnetized and non-magnetized hulless barley seeds across physiological, transcriptomic, hormonal, and agronomic levels. Multi-omics analysis revealed that magnetic field treatment acts as a systemic priming cue that temporally coordinates redox homeostasis, carbon-energy metabolism, and phytohormone signaling. The most pronounced transcriptional and hormonal reorganization occurred at 12 h post-imbibition, a critical window characterized by concurrent activation of auxin, gibberellin, and cytokinin pathways, suppression of ABA signaling, enhanced antioxidant defense, and accelerated starch mobilization. These coordinated changes were not attributable to a single dominant pathway; rather, they reflect a network-level reprogramming that collectively accelerates dormancy release, radicle emergence, and early seedling growth. Importantly, these early physiological and molecular advantages translated into improved field establishment and consistent

553 grain yield increases of 6.81% in 2025 ($P < 0.05$) and 5.35% in 2026 ($P < 0.01$) under
554 plateau conditions. Collectively, these findings document that magnetic-field priming
555 is associated with enhanced hulless barley germination and productivity, accompanied
556 by coordinated shifts in antioxidant defense, carbon-energy metabolism, and
557 growth-promoting hormone signalling, as well as stage-specific transcriptional
558 reprogramming.

559 **4.1 Magnetic field treatment establishes the physiological foundation for**
560 **germination through synergistic optimization of antioxidant defense and**
561 **carbon–energy metabolism**

562 Elevated CAT, SOD, POD, and GPx activities alongside reduced MDA content
563 were observed under magnetic priming, consistent with enhanced antioxidant defence
564 and alleviated membrane lipid peroxidation [25]. Notably, H_2O_2 tended to be higher
565 in the CH group at 0 h, before imbibition, and was significantly higher at 12 h and 24
566 h, suggesting that magnetic treatment altered the seed redox state prior to and during
567 early imbibition. We speculate that H_2O_2 in CH was not eliminated but maintained at
568 a signaling concentration, consistent with the concept that moderate ROS supports
569 signaling while avoiding oxidative damage [26]. Similar protective effects have been
570 observed in mungbean seedlings under heavy metal stress [27]. The direction of H_2O_2
571 change under magnetic treatment is species- and parameter-dependent; increased
572 H_2O_2has been reported in cucumber [28] and broad bean [29]. In our study, CH
573 maintained higher H_2O_2 but lower MDA and higher antioxidant enzyme activities,

suggesting that H_2O_2 was kept at a signaling level rather than causing oxidative damage.

At the energy metabolism level, magnetic treatment significantly increased α-amylase activity and accelerated starch degradation. Although soluble sugar content in CH was slightly lower than in CK, ATP content was continuously elevated, indicating that carbon flux shifted from storage decomposition toward energy synthesis. Sugars derived from starch degradation were rapidly utilized for ATP production to meet the energy demands of cell division and organ growth. This pattern aligns with findings in cumin, sunflower, and marigold [30-33] and with the enhanced α-amylase activity and accelerated starch degradation reported in magnetically treated brown rice [22, 34-37]. The magnitude of antioxidant enzyme changes observed here is comparable to previous studies, in which CAT activity increased by 64.0% in Bupleurum chinense [38] and SOD activity increased by up to 321% in black soybean [39]. Collectively, these physiological observations show coordinated shifts in antioxidant defense and carbon-energy metabolism that may underlie the observed germination-performance differences between treatments.

4.2 Stage-specific transcriptional reprogramming induced by magnetic treatment mirrors germination progression

Transcriptome analysis revealed that the transcriptional response to magnetic treatment was highly stage-specific: the CH vs CK DEG sets differed among germination time points, with few or no shared DEGs among time points. Such temporal and dose dependence is consistent with the duration-dependent germination

responses reported for dynamic magnetic field exposure in rice [40] and with the improved germination and vigour of accelerated-aged seeds under low-frequency magnetic field [41], supporting the view that the effectiveness of magnetic treatment depends on matching the field dose to the specific stage of imbibition and germination. Such rapid and stage-specific transcriptome reprogramming is consistent with the 394 and 168 DEGs identified in shoots and roots of Arabidopsis under static magnetic field [24], and with the improved germination of Acacia cinnamata seeds under magnetic field [42].

At 0 h, magnetic treatment-induced DEGs were enriched in membrane reconstruction and osmotic regulation pathways, suggesting molecular differences related to membrane reconstruction and osmotic regulation emerge at early imbibition under magnetic priming. At 12 h, the transcriptional response was most intense. DEGs were enriched in cell cycle, starch–sucrose metabolism, and amino acid metabolism pathways, consistent with the increased demand for cell proliferation and efficient energy metabolism during the transition from dormancy to germination. The strong enrichment of starch and sucrose metabolism at 12 h is supported by [22], who reported that magnetic treatment combined with gibberellin up-regulated OsAmy1A, OsAmy1C, OsAmy3C and OsAmy3E by 331.4%, 148.6%, 375.7% and 47.9% within 36 h in brown rice.

At 24 h, the photosynthesis-antenna proteins pathway was significantly enriched for the first time, marking the early initiation of autotrophic system assembly. Similar early activation of photosynthetic and antioxidant pathways has been observed in

magnetically treated soybean [23], Arabidopsis [24], and wheat [43]. At 48 h, development related genes were up-regulated, while stress response genes were down-regulated, reflecting the coordination of growth and defense resource allocation by magnetic field treatment. At 72 h, pathways related to photosynthetic carbon fixation and organ development were enriched, indicating that seedlings had entered the differentiation and maturation stage, with transcriptional regulation shifting toward improved photosynthetic efficiency and maintenance of meristem activity.

4.3 Magnetic treatment-induced temporal reorganization of the hormone signaling network drives dormancy release and growth promotion

Hormone pathways regulate seed germination through synergistic and antagonistic interactions. Here, magnetic treatment regulated the hormone signaling network in a pathway-specific and temporally dynamic manner, with the most pronounced changes occurring at 12 h post-imbibition, coinciding with the peak transcriptional response. This temporal alignment is consistent with hormone network reorganization being a component of the synchronized multi-level response to magnetic treatment.

Auxin, cytokinin, brassinosteroid, and gibberellin pathways were synergistically activated. The auxin pathway showed upregulation across the entire cascade from carrier uptake to Aux/IAA early response genes, which in turn activated downstream auxin signaling. This is consistent with findings in Arabidopsis, where static magnetic field regulated root elongation by modulating the expression of auxin transporter proteins PIN3 and AUX1 [18]. The cytokinin and brassinosteroid pathways jointly

activated cell cycle-related genes, with ARR-A and BAK1 showing 2.83- and 3.2-fold increases in CH relative to CK at 12 h, respectively, converging on CyclinD3 to promote cell division. In the gibberellin pathway, DELLA, a core negative regulator, was downregulated by 67% in CH relative to CK at 12 h, while GA_{20} and GA_7 began accumulating at 0 h and continued through 24 h. These DELLA-related transcriptional changes and GA accumulation are consistent with altered GA-associated regulation. Collectively, these expression and metabolite shifts are consistent with relief of gibberellin-signalling repression and enhanced potential for cell elongation. Rapid hormone changes within 12 h of imbibition are supported by [44], who showed that magnetic treatment at 12 h after imbibition increased NO and decreased ABA in Paulownia elongata seeds. In magnetically treated brown rice, endogenous GA increased by 33.45% and α-amylase genes were strongly up-regulated within 36 h [22].

ABA-related genes showed transcriptional changes. At the hormone level, ABA decreased at 12 h, while the ethylene precursor ACC synchronously increased. At the gene level, PP2C was downregulated by 64%, and the ABA receptor PYL and kinase SRK2 were downregulated by 74% in CH relative to CK at 12 h, collectively indicating transcriptional changes in ABA-related signaling. The concurrent DELLA downregulation and downregulation of ABA signaling genes (PP2C, PYL, and SRK2) are consistent with altered regulation of seed dormancy. This GA–ABA antagonistic pattern is consistent with findings in faba bean and pea [45, 46] and with the role of H_2O_2 in mediating ABA catabolism and GA biosynthesis in Arabidopsis seeds [47]. In

maize seedlings, magnetic treatment promoted salicylic acid synthesis at 24 h and inhibited ABA at 72 h, while jasmonic acid showed the opposite trend [48].

An important finding of this study is that the JA/SA defense pathways in hulless barley exhibited a dynamic temporal pattern distinct from that reported in wheat. In wheat, magnetic treatment continuously suppresses jasmonic acid biosynthesis through TaHY5 [19]. In contrast, hulless barley showed early suppression of JA/SA signaling during germination initiation, followed by moderate activation at mid- to late stages to establish defense capacity, with PR-1 genes specifically induced at 24 h. This difference suggests that crop species may adopt distinct defense strategies in response to magnetic treatment, and the underlying mechanisms warrant further investigation. Together, these hormone dynamics indicate that magnetic field treatment is associated with changes in the phytohormone network, including changes in growth-promoting pathways and ABA-related signaling, which are consistent with accelerated dormancy release and seedling growth.

4.4 From hormone dynamics to field yield: an integrated chain and candidate magneto-perception modules

The pronounced stage-specific transcriptional reprogramming prompted us to ask whether any candidate magneto-perception modules could be inferred from the transcriptome. Before turning to these speculative candidates, it is worth noting that while the core GA/ABA antagonistic pattern is conserved across species, the JA/SA response in hulless barley showed a distinct temporal pattern—early suppression followed by moderate activation at 48–72 h—which differs from the continuous JA

suppression reported in wheat [19]. This suggests that the downstream defense–growth trade-off may be species-specific even when the core hormone network is conserved.

Beyond the hormone network itself, the present dataset allows a more direct link between early molecular events and the field yield gain. The 12-h transcriptome was dominated by starch and sucrose metabolism (fold = 15.27), and this transcriptional signal was mirrored at the biochemical level by a 30.7% increase in α-amylase activity at 48 h and a 13.8% increase in ATP at 24 h, with soluble sugar remaining slightly lower in CH—i.e., carbon flux was directed toward energy production rather than accumulating as soluble sugar. This energy supply coincides temporally with the GA/ABA shift (DELLA downregulation at 12 h, GA accumulation through 24 h, ABA decline at 12 h), which together would be expected to lower the dormancy barrier and fuel radicle emergence. The phenotypic consequence was a 43.6% higher root formation rate at 24 h and a 57.2% higher root length at 96 h. At the field level, the same treatment produced 8.56% (2025) and 4.63% (2026) higher emergence and 7.86%/11.22% higher effective panicle density, which translated into 6.81% and 5.35% yield gains. The yield pathway was "spike-number-dominant, grain-number-supplementary, with a slight grain-weight penalty," consistent with the early establishment advantage being carried through to the population level. While these links remain correlative, they form a coherent chain—starch mobilization → ATP supply → GA/ABA-mediated dormancy release → radicle/root growth → field

705 establishment → panicle number → yield—that is supported at every level by
706 independent measurements in this study.

707 Finally, the transcriptome data point to two candidate modules that may be worth
708 testing in future functional work: HY5 was up-regulated at 12 h while COP1 was
709 down-regulated, and several Fe–S cluster assembly genes (ISU1, HCF101, NAR1,
710 SDH) showed stage-specific expression changes. Because HY5 can bind the $GA_{20}ox$
711 promoter in Arabidopsis [49], and Fe–S clusters are redox-sensitive components of
712 mitochondrial energy metabolism [50], these observations are compatible with a
713 hypothetical HY5–GA and Fe–S–energy link to the physiological changes described
714 above. However, we did not measure tissue iron content, nor did we perform any
715 genetic perturbation in hulless barley; these modules should therefore be regarded
716 strictly as hypothesis-generating observations, not as validated magneto-perception
717 mechanisms. They are reported here to provide a prioritized starting point for future
718 genetic-functional studies rather than as an explanatory model for the present data.

719 **4.5 Application potential and perspectives**

720 From an agronomic perspective, magnetically induced improvements in
721 germination uniformity, seedling vigor, and root system development are generally
722 associated with final yield in cereal crops. The enhanced energy metabolism and
723 rebalanced hormone network during early establishment may provide a physiological
724 foundation for better resource capture and stress resilience under field conditions.
725 Consistent with this, pre-sowing magnetic treatment increased plant growth and yield
726 in tomato [51] and, in field studies in China, raised wheat yield through improved root

activity and nutrient uptake [11]. Magnetic treatment has been reported to increase wheat, rice and rapeseed yield by 8.3–10.9%, 10.0–25.3% and 9.07–9.43%, respectively [52], consistent with the 5.35–6.81% yield gains observed here.

Beyond yield, magnetic treatment is increasingly regarded as a tool for improving stress tolerance. Magnetopriming or magnetised-water irrigation can mitigate the adverse effects of salinity and drought, as demonstrated in tomato under salinity stress [53] and in annual medic under combined salt–drought stress [54]. This suggests that magnetic seed priming could be integrated into management practices for marginal and saline soils, complementing the benefits observed here for hulless barley. Other physical priming approaches have shown similar benefits. Pulsed electric field treatment improved soybean germination index by 35.18% and stem length by 40.4% under normal conditions and alleviated salt and drought stress [55]. Pulsed high-intensity magnetic field treatment also improved wheat seed germination [56]. However, because the optimal field intensity and exposure duration are species- and even cultivar-specific [7], the treatment conditions established in this study cannot be directly transferred to other crops without systematic screening.

Mechanistically, the perception and transduction of magnetic signals remain poorly understood. The candidate modules proposed here—HY5 and Fe-S cluster homeostasis—were inferred from transcriptome data alone and should be considered as candidate hypotheses for future functional studies. In addition, whether the transcriptional and hormonal reprogramming observed at the germination stage persists into later developmental stages, and how it interacts with genotype and

environment, remain open questions. Future studies will conduct multi-year, multi-location field trials to validate the long-term agronomic performance of magnetic seed priming in hulless barley and provide direct evidence for the adoption of magnetic field technology in sustainable agriculture on the Qinghai–Tibet Plateau.

5. Conclusion

In summary, four-stage dynamic pulsed magnetic-field priming (50-150 mT, total 17 min) was associated with wide-ranging physiological, transcriptomic and phytohormone alterations in germinating hulless-barley seeds. Priming coincided with elevated antioxidant-enzyme activities, transient signalling-level accumulation of H_2O_2 (most prominent at 12 h and 24 h), reduced MDA concentration, and increased α-amylase and ATP levels. Transcriptomic analysis uncovered 7414 DEGs at 12 h post-imbibition, with starch-and-sucrose metabolism as the top enriched pathway. Targeted hormone profiling demonstrated coordinated shifts in auxin, gibberellin, cytokinin and brassinosteroid-associated pathways alongside modified ABA-related signalling, changes consistent with accelerated dormancy release and early seedling establishment. Two-consecutive-year field trials showed improved seedling emergence, higher effective panicle density and more grains per spike, producing averaged yield gain of 6.10 %, offsetting a small reduction in thousand-grain weight.

It should be emphasised that the molecular regulatory relationships reported in this work are correlative rather than proven causal interactions. Candidate genes and speculative magneto-perception hypotheses (HY5-related cascade and Fe-S-cluster

homeostasis) deduced from transcriptome data await rigorous genetic-functional testing. Collectively, our work supplies multi-omics resources and multi-year agronomic evidence supporting dynamic pulsed magnetic priming as a promising physical seed-treatment technique for hulless-barley production on the Qinghai-Tibet Plateau.

Declarations

Ethics approval and consent to participate

Not applicable.

Consent for publication

Not applicable.

Competing interests

The authors declare that they have no known competing financial interests or personal relationships that could have appeared to influence the work reported in this paper. The commercial affiliations of Yu Lin (Qinghai Miche Agricultural and Animal Husbandry Technology Co., Ltd.) and Ping Ma (Qinghai Tianyoude Technology Investment Management Group Co., Ltd.) did not influence the study design, data collection, analysis, or interpretation.

Funding

This work was supported by the National Key Research and Development Program of China (Grant No. 2022YFD2301305).

Authors' contributions

H.W. and X.Y. conceived and designed the study. H.W. performed the experiments, analyzed the data, and wrote the original draft. X.Y. supervised the project, acquired funding, and revised the manuscript. Y.L. and P.M. provided resources and contributed to the review and editing of the manuscript. All authors read and approved the final manuscript.

Availability of data and materials

Raw sequence data for 28 of the 30 samples reported in this study have been deposited in the Genome Sequence Archive (GSA) in the National Genomics Data Center, China National Center for Bioinformation / Beijing Institute of Genomics, Chinese Academy of Sciences, under accession number CRA046706, publicly accessible at https://ngdc.cncb.ac.cn/gsa. Due to an unforeseen hard-drive failure during post-analysis data archiving, the raw FASTQ files for two biological replicates of the 12-h control group (K12_rep2 and K12_rep3) were corrupted and could not be recovered despite our best efforts, including contacting the sequencing facility. Consequently, the GSA repository contains raw reads for 28 samples (56 paired-end files) rather than the full set of 30 samples.

All transcriptomic analyses presented in this study, including DEG identification, hormone–gene correlation, and field-data analysis, were completed before the data loss and were based on the complete 30-sample dataset with three biological

replicates per time point. The expression values for K12_rep2 and K12_rep3 are included in the complete FPKM expression matrix for all 30 samples, which has been deposited in Figshare under DOI: 10.6084/m9.figshare.33040364 (https://figshare.com). This matrix is provided to support independent verification of the expression-based analyses. We apologize for this unavoidable data loss and remain fully committed to data transparency and scientific rigor.

In addition, the raw count matrix, sample metadata, and all analysis scripts used for DEG identification, hormone-gene correlation, and field-data mixed-model analysis have been deposited in Figshare under the same DOI.

References

1. Yangjin L. Effect of different fertilization modes on yield and quality of Tibetan highland barley. Chin Agric Knowl Warehouse. 2025;21(6):55-8. Chinese.
2. Hu Y. Pathways and roles of promoting highland barley planting technology in alpine regions. Seed Sci Technol. 2024;42:62-4. https://doi.org/10.19904/j.cnki.cn14-1160/s.2024.02.021
3. Rani L, Thapa K, Kanojia N, Sharma N, Singh S, et al. An extensive review on the consequences of chemical pesticides on human health and environment. J Clean Prod. 2021;283:124657. https://doi.org/10.1016/j.jclepro.2020.124657
4. Xu Q. Contamination characteristics of typical pollutants in soil-vegetable systems and physiological effects of antibiotics [Doctoral dissertation]. Zhejiang University; 2019.

5. Mahajan TS, Pandey OP. Magnetic-time model at off-season germination. Int Agrophys. 2014;28:57-62. https://doi.org/10.2478/intag-2013-0027

6. Haq Z, Iqbal M, Jamil Y, Anwar H, Younis A, Arif M, et al. Magnetically treated water irrigation effect on turnip seed germination, seedling growth and enzymatic activities. Inf Process Agric. 2016;3:99-106. https://doi.org/10.1016/j.inpa.2016.03.004

7. Xia X, Pagano A, Macovei A, Padula G, Balestrazzi A, Holubowicz R. Magnetic field treatment on horticultural and agricultural crops: Its benefits and challenges. Folia Hortic. 2024a;36:67-80. https://doi.org/10.2478/fhort-2024-0004

8. Bukhari SA, Tanveer M, Mustafa G, Zia-Ud-Den N. Magnetic field stimulation effect on germination and antioxidant activities of presown hybrid seeds of sunflower and its seedlings. J Food Qual. 2021;2021:5594183. https://doi.org/10.1155/2021/5594183

9. Ali KA, El-Tayeb MA, Al-Qahtani WH, et al. Pre-sowing magnetic stimulation enhanced germination and growth attributes of maize (*Zea mays*) seed. Pol J Environ Stud. 2026;35:3031. https://doi.org/10.15244/pjoes/203577

10. Asghar T, Iqbal M, Jamil Y, Zia-ul-Haq, Nisar J, Shahid M. Comparison of He-Ne laser and sinusoidal non-uniform magnetic field seed pre-sowing treatment effect on *Glycine max* (Var 90-I) germination, growth and yield. J Photochem Photobiol B Biol. 2017;166:212-9. https://doi.org/10.1016/j.jphotobiol.2016.11.018

11. Zhang Y, Dou H, Yang L, Zhang Y, Sun W, Ruan Y, et al. Innovative approach to utilising magnetic fields to enhance wheat yield: Evidence from field studies in China. Plant Soil Environ. 2024;70:656-72. https://doi.org/10.17221/285/2024-PSE
12. Abdolmaleki P, Ghanati F, Sahebjamei H, Sarvestani AS. Peroxidase activity, lignification and promotion of cell death in tobacco cells exposed to static magnetic field. Environmentalist. 2007;27:435-40. https://doi.org/10.1007/s10669-007-9080-1
13. Mahdigholi K, Volkov DS, Kuznetsov VV. Effects of static magnetic fields on the antioxidant system of almond seeds. Russ J Plant Physiol. 2019;66:299-307. https://doi.org/10.1134/S102144371902002X
14. Afzal I, Mukhtar K, Qasim M, Basra SMA, Shahid M, Haq Z. Magnetic stimulation of marigold seed. Int Agrophys. 2012;26:335-9. https://doi.org/10.2478/v10247-012-0047-1
15. Xu C, Yin X, Lv Y, Wu C, Zhang Y, Song T. A near-null magnetic field affects cryptochrome-related hypocotyl growth and flowering in *Arabidopsis*. Adv Space Res. 2012;49:834-40. https://doi.org/10.1016/j.asr.2011.12.004
16. Xu C, Lv Y, Chen C, Zhang Y, Wei S. Blue light-dependent phosphorylations of cryptochromes are affected by magnetic fields in *Arabidopsis*. Adv Space Res. 2014;53:1118-24. https://doi.org/10.1016/j.asr.2014.01.033

17. Xu C, Yu Y, Zhang Y, Li Y, Wei S. Gibberellins are involved in effect of near-null magnetic field on *Arabidopsis* flowering. Bioelectromagnetics. 2017;38:1-10. https://doi.org/10.1002/bem.22004
18. Jin Y, Guo W, Hu X, Liu M, Xu X, Hu F, et al. Static magnetic field regulates *Arabidopsis* root growth via auxin signaling. Sci Rep. 2019;9:14384. https://doi.org/10.1038/s41598-019-50970-y
19. Li Z, Gao J, Mu W, Wang C, Lin X, Wang Z, et al. Static magnetic field promotes wheat nitrogen assimilation by repressing jasmonates biosynthesis through TaHY5. Plant Biotechnol J. 2025. https://doi.org/10.1111/pbi.70360
20. Zhang HL. Study on cold resistance of Xanthoceras sorbifolia in alpine regions [Master's thesis]. Mudanjiang Normal University; 2024. https://doi.org/10.27757/d.cnki.gmdjs.2024.000405
21. Ramalingam R. Seed pretreatment with magnetic field alters the storage proteins and lipid profiles in harvested soybean seeds. Physiol Mol Biol Plants. 2018;24:343-7. https://doi.org/10.1007/s12298-018-0505-8
22. Han L, Wang G, Cao H, Xu H, Sun H, Cai L, et al. Effect of magnetic field treatment on the nutritional quality and antioxidant activity of germinated brown rice. Food Biosci. 2024;62:105510. https://doi.org/10.1016/j.fbio.2024.105510
23. Baghel L, Kataria S, Guruprasad KN. Effect of static magnetic field pretreatment on growth, photosynthetic performance and yield of soybean under water stress. Photosynthetica. 2018;56:718-30. https://doi.org/10.1007/s11099-017-0722-3

24. Zhou X, Zhang L, Zhang P, et al. Comparative transcriptomic analysis revealed important processes underlying the static magnetic field effects on *Arabidopsis*. Front Plant Sci. 2024;15:1390031. https://doi.org/10.3389/fpls.2024.1390031
25. Tang P, Chen Z. Effects of different magnetic fields on germination and growth of *Pisum sativum*. J Anhui Agric Sci. 2021;49:38-40.
26. Shine MB, Guruprasad KN, Anand A. Effect of stationary magnetic field strengths of 150 and 200 mT on reactive oxygen species production in soybean. Bioelectromagnetics. 2012;33:428-37. https://doi.org/10.1002/bem.21702
27. Chen Y, Li R, He J. Magnetic field can alleviate toxicological effect induced by cadmium in mungbean seedlings. Ecotoxicology. 2011;20:760-9. https://doi.org/10.1007/s10646-011-0620-6
28. Bhardwaj J, Anand A, Nagarajan S. Biochemical and biophysical changes associated with magnetopriming in germinating cucumber seeds. Plant Physiol Biochem. 2012;57:67-73. https://doi.org/10.1016/j.plaphy.2012.05.008
29. Jouni FJ, Abdolmaleki P, Ghanati F. Oxidative stress in broad bean (*Vicia faba L.*) induced by static magnetic field under natural radioactivity. Mutat Res. 2012;741:116-21. https://doi.org/10.1016/j.mrfmmm.2012.03.005
30. Asadi Samani M, Pourakbar L, Azimi N. Magnetic field effects on seed germination and activities of some enzymes in cumin. Life Sci J. 2013;10. https://doi.org/10.7537/marslsj100113.53

31. Ananta V, Nagarajan S. Exposure of seeds to static magnetic field enhances germination and early growth characteristics in chickpea (*Cicer arietinum L.*). Bioelectromagnetics. 2008;29:571-8. https://doi.org/10.1002/bem.20426

32. Ananta V, Nagarajan S. Effect on germination and early growth characteristics in sunflower (*Helianthus annuus*) seeds exposed to static magnetic field. J Plant Physiol. 2009;167:149-56. https://doi.org/10.1016/j.jplph.2009.08.011

33. Afzal I, Saleem S, Skalicky M, Javed T, Bakhtavar MA, Haq Z, et al. Magnetic field treatments improves sunflower yield by inducing physiological and biochemical modulations in seeds. Molecules. 2021;26:2022. https://doi.org/10.3390/molecules26072022

34. Luo X, Li R, Huang J, Chen Y, Zhang S. Static magnetic field treatment improves starch properties and glycemic response of brown rice: A multi-omics study. Food Chem. 2022;383:132392. https://doi.org/10.1016/j.foodchem.2022.132392

35. Chen CW, Tao Y, Han YB, et al. Preparation of germinated brown rice with high γ-aminobutyric acid content and short root by magnetic field treatment. J Cereal Sci. 2023;112:103720. https://doi.org/10.1016/j.jcs.2023.103720

36. Luo X, Tao Y, Han Y, et al. Effect of static magnetic field treatment on γ-aminobutyric acid content and sensory characteristics of germinated brown rice cake. Food Chem. 2023;404:134709. https://doi.org/10.1016/j.foodchem.2022.134709

939 37. Jiang X, Zheng F, Yu J, Lv P, Ban H, Liu H, et al. Effects of static magnetic field
940 treatment on the digestive, structural and physicochemical characteristics of
941 germinated corn starch. Food Chem. 2025;470:142670.
942 https://doi.org/10.1016/j.foodchem.2024.142670
943 38. Zhang R, Yuan X, Zou H, Gao Y, Qin H. Effects of magnetic field on seed
944 germination and seedling stress resistance of Bupleurum chinense. Chin Agric
945 Sci Bull. 2019;36:50-4.
946 39. Tang P, Long Y. Effect of magnetic field on the germination and growth of
947 Glycine max var. Tillage and Cultivation. 2021;41:43-6.
948 40. Gaewsondee T, Chiawchanwattana C, Khaengkhan P, Laohavanich J,
949 Vipattanaporn C, Yangyuen S. Influence of dynamic magnetic field exposure
950 duration on the germination and growth of Khao Dawk Mali 105 rice seed.
951 Agronomy. 2025;15:1630. https://doi.org/10.3390/agronomy15071630
952 41. Xia X, Zając-Woźnialis A, Padula G, Kubisz L, Hołubowicz R. Effect of low
953 frequency magnetic field (LFMF) on germination and vigour of accelerated aged
954 radish (*Raphanus sativus L.*) seeds. Folia Hortic. 2024b;36:425-34.
955 https://doi.org/10.2478/fhort-2024-0027
956 42. Zhou Y, Wei X, Zhu M, Chen L, Rong J, Zheng Y. Effect of magnetic field on
957 seed germination and physiological and biochemical properties of *Acacia*
958 *cincinnata*. J Fujian Agric For Univ (Nat Sci Ed). 2026;55:525-34.
959 43. Zheng S, Xu J. Effect of magnetic treatment on seed germination and
960 photosynthetic characteristics of wheat. J Triticeae Crops. 2010;30:79-82.

961 44. Liu J. Effects of magnetic field on seed dormancy and germination of Paulownia
962 elongata and its mechanism [Doctoral dissertation]. Nanjing Forestry University;
963 2019.
964 45. Podlesna A, Podlesny J, Gladyszewska B. Effect of pre-sowing magnetic field
965 treatment on some biochemical and physiological processes in faba bean (*Vicia*
966 *faba L. spp. Minor*). J Plant Growth Regul. 2019;38:1153-60.
967 https://doi.org/10.1007/s00344-019-09920-1
968 46. Podlesny J, Podlesna A, Gladyszewska B, Bojarszczuk J. Effect of pre-sowing
969 magnetic field treatment on enzymes and phytohormones in pea (*Pisum sativum*
970 *L.*) seeds and seedlings. Agronomy. 2021;11:494.
971 https://doi.org/10.3390/agronomy11030494
972 47. Liu Y, Ye N, Liu R, Chen M, Zhang J. H2O2 mediates the regulation of ABA
973 catabolism and GA biosynthesis in *Arabidopsis* seed dormancy and germination.
974 J Exp Bot. 2010;61(11):2979-90. https://doi.org/10.1093/jxb/erq125
975 48. Zheng B. Effects of magnetic field on growth and development of maize
976 seedlings [Master's thesis]. Henan Agricultural University; 2018.
977 49. Lee J, He K, Stolc V, Lee H, Figueroa P, Gao Y, et al. Analysis of transcription
978 factor HY5 genomic binding sites revealed its hierarchical role in light regulation
979 of development. Plant Cell. 2007;19:731-49.
980 https://doi.org/10.1105/tpc.106.047688

50. Balk J, Pilon M. Ancient and essential: The assembly of iron-sulfur clusters in plants. Trends Plant Sci. 2011;16:218-26. https://doi.org/10.1016/j.tplants.2010.12.006

51. De Souza A, García D, Sueiro L, Gilart F, Porras E, Licea L. Pre-sowing magnetic treatments of tomato seeds increase the growth and yield of plants. Bioelectromagnetics. 2006;27:247-57. https://doi.org/10.1002/bem.20206

52. Zhang J, Hu L. The progress of crops seed treatment. J Huazhong Agric Univ. 2012;31:258-64.

53. Samarah NH, Bany Hani MMI, Makhadmeh IM. Effect of magnetic treatment of water or seeds on germination and productivity of tomato plants under salinity stress. Horticulturae. 2021;7:220. https://doi.org/10.3390/horticulturae7080220

54. Sharafi S. Combined ultrasound and magnetic field treatment improves salt and drought tolerance in annual medic (*Medicago scutellata L.*) seeds. Appl Water Sci. 2025;15:59. https://doi.org/10.1007/s13201-025-02121-x

55. Liu L. Mechanism study on the effects of pulsed electric fields on soybean seed germination and physiological processes [Master's thesis]. Hubei University of Technology; 2026.

56. Shen Z. Experimental study on the effects of high-intensity pulsed magnetic field on wheat seed germination and Rhizoctonia solani [Master's thesis]. Nanjing Agricultural University; 2017.

57. National Genomics Data Center. Database Resources of the National Genomics Data Center, China National Center for Bioinformation in 2026. Nucleic Acids Res. 2026;54:D28-47. https://doi.org/10.1093/nar/gkaf1172

Figure and Table legends

Fig. 1 Effects of magnetic field treatment on hulless barley seed germination and seedling growth. (A) Bud weight; (B) Root number; (C) Bud length; (D) Root length; (E) Germination rate; (F) Root formation rate; (G) Stored substance transport rate, relative water content, germination energy, germination index, root-shoot ratio, and vigor index; (H) Seed germination and seedling growth phenotypes. Germination rate and root formation rate n=500, with bud or root ≥2 mm counted as germinated (or rooted); other phenotype indicators n=30, scale bar = 1 cm. Different lowercase letters indicate significant differences among time points within the same treatment ($P < 0.05$); * indicates $P < 0.05$, ** indicates $P < 0.01$. CK: non-magnetized group; CH: magnetic field treatment group.

Fig. 2 Effects of magnetic field treatment on physio-biochemical characteristics during hulless barley seed germination. (A) CAT activity; (B) SOD activity; (C) POD activity; (D) GPx activity; (E) MDA content; (F) H_2O_2 content; (G) α-amylase activity; (H) ATP content; (I) Soluble sugar content; (J) Soluble protein content; (K) Free proline content. Different lowercase letters indicate significant differences among time points within the same treatment ($P < 0.05$); * indicates $P < 0.05$, ** indicates $P < 0.01$. CK: non-magnetized group; CH: magnetic field treatment group**.**

Fig. 3 Overall transcriptome analysis of hulless barley seed germination under magnetic field treatment. (A) Principal component analysis (PCA); (B) Venn diagram of differentially expressed genes; (C) Statistics of differentially expressed gene numbers.

Fig.4 Hormone signaling pathway network regulated by magnetic field treatment during hulless barley seed germination. The heatmap was drawn based on FPKM values (FPKM > 10), with red indicating high expression and green indicating low expression.

Fig. 5 Heatmap of differential hormone contents during hulless barley seed germination under magnetic field treatment. (A) Statistics of the number of differential hormones; (B) K0 vs H0; (C) K12 vs H12; (D) K24 vs H24; (E) K48 vs H48; (F) K72 vs H72. Red indicates high expression, blue indicates l ow expression.

Fig. 6 qRT-PCR validation of key hormone signaling genes. Five hormone-related genes were selected for qRT-PCR verification across five germination time points (0, 12, 24, 48, and 72 h). Light blue and dark blue bars represent qRT-PCR relative expression of CK and CH treatments, respectively. Relative expression was calculated using the $2^{-\Delta\Delta Ct}$ method; for each time point, the mean ΔCt of the non-magnetized control (CK) was used as the calibrator (set to 1.0). The only exception was IAA at 0 h, for which CK expression was below the qPCR detection limit (Ct > 35); therefore, no CK calibrator was defined, and IAA validation was restricted to 12–72 h. Green circles and orange squares indicate FPKM values of CK and CH treatments from transcriptome sequencing (mean ± SD, n = 3). Error bars represent standard deviation. Asterisks above the CH bars indicate significant differences between CK and CH treatments (* $p < 0.05$, ** $p < 0.01$, *** $p < 0.001$, **** $p < 0.0001$; ns: not significant). Gene abbreviations: IAA, auxin-responsive protein gene (HORVU.MOREX.r3.5HG0509760); ARR-A, two-component response regulator ARR-A family gene (HORVU.MOREX.r3.3HG0321410); DELLA, DELLA protein gene (HORVU.MOREX.r3.2HG0130900); ABF, ABA-responsive element binding factor gene (HORVU.MOREX.r3.3HG0300770); NPR1, regulatory protein NPR1 gene (HORVU.MOREX.r3.2HG0214180).

Fig. 7 Gene–hormone–physiological indicator association network analysis. (A) Overall correlation heatmap; (B) Correlation heatmap of the control group (CK); (C) Correlation heatmap of the magnetized treatment group (CH); (D-G) Li near fitting of key indicators: (D) Gibberellin GA_{20} content vs. SOD activity, R^2 = 0.931 for CH group, R^2 = 0.805 for CK group; (E) Abscisic acid content vs. A

TP content; (F) NPR1 gene expression vs. salicylic acid content; (G) Jasmonic acid content vs. proline content. Scatter points represent individual samples, lines indicate linear fitting, and shaded areas represent the 95% confidence interval. The barley gene IDs shown in the figure are abbreviated forms derived from the Morex v3 reference genome (HORVU.MOREX.r3). Full gene IDs and detailed functional annotations are provided in Supplementary Table S4 (e.g., HORVU.MOREX.r3.5HG0509760 appears as 5HG0509760 in the Fig. 7A-7C).

Table 1 Effects of magnetic field treatment on field establishment, yield components, and grain yield of hulless barley in 2025 and 2026.

Figure 1

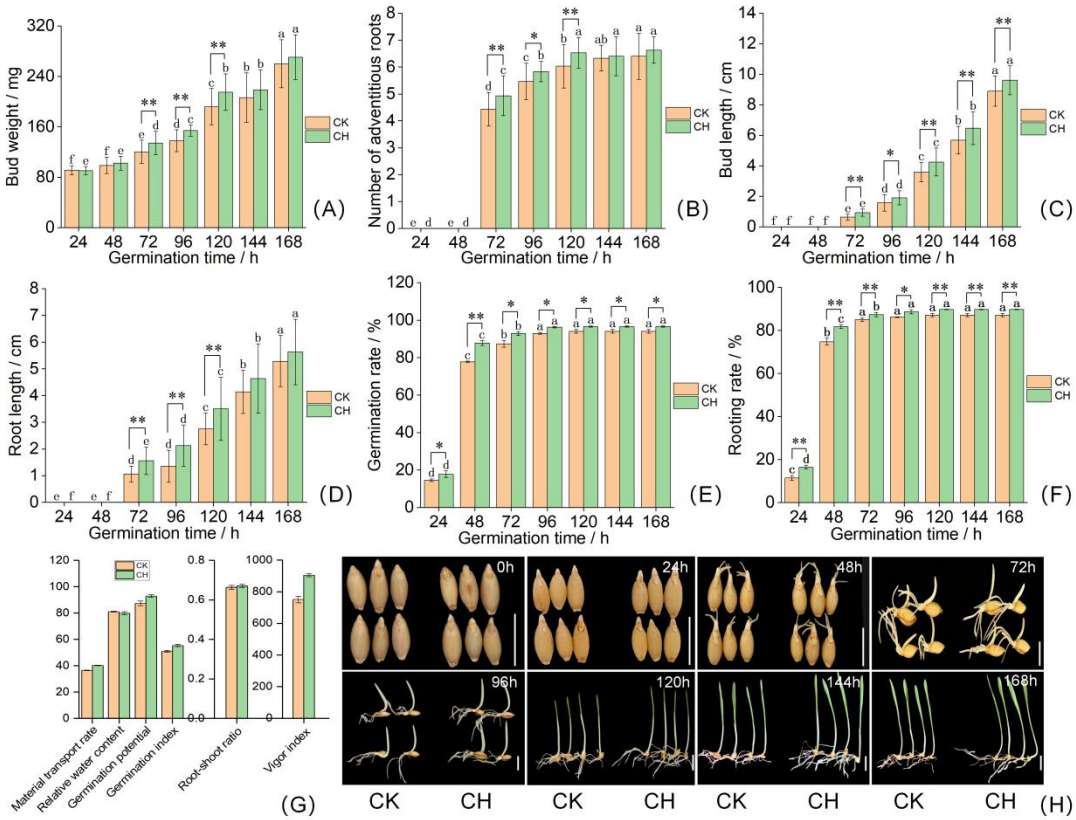

Bud weight / mg
Germination time / h
(A)
Number of adventitious roots
(B)
Bud length / cm
(C)
Root length / cm
(D)
Germination rate / %
(E)
Rooting rate / %
(F)
CK
CH
Material transport rate
Relative water content
Germination potential
Germination index
Root-shoot ratio
Vigor index
(G)
0h
24h
48h
72h
96h
120h
144h
168h
CK
CH
(H)

Figure 2

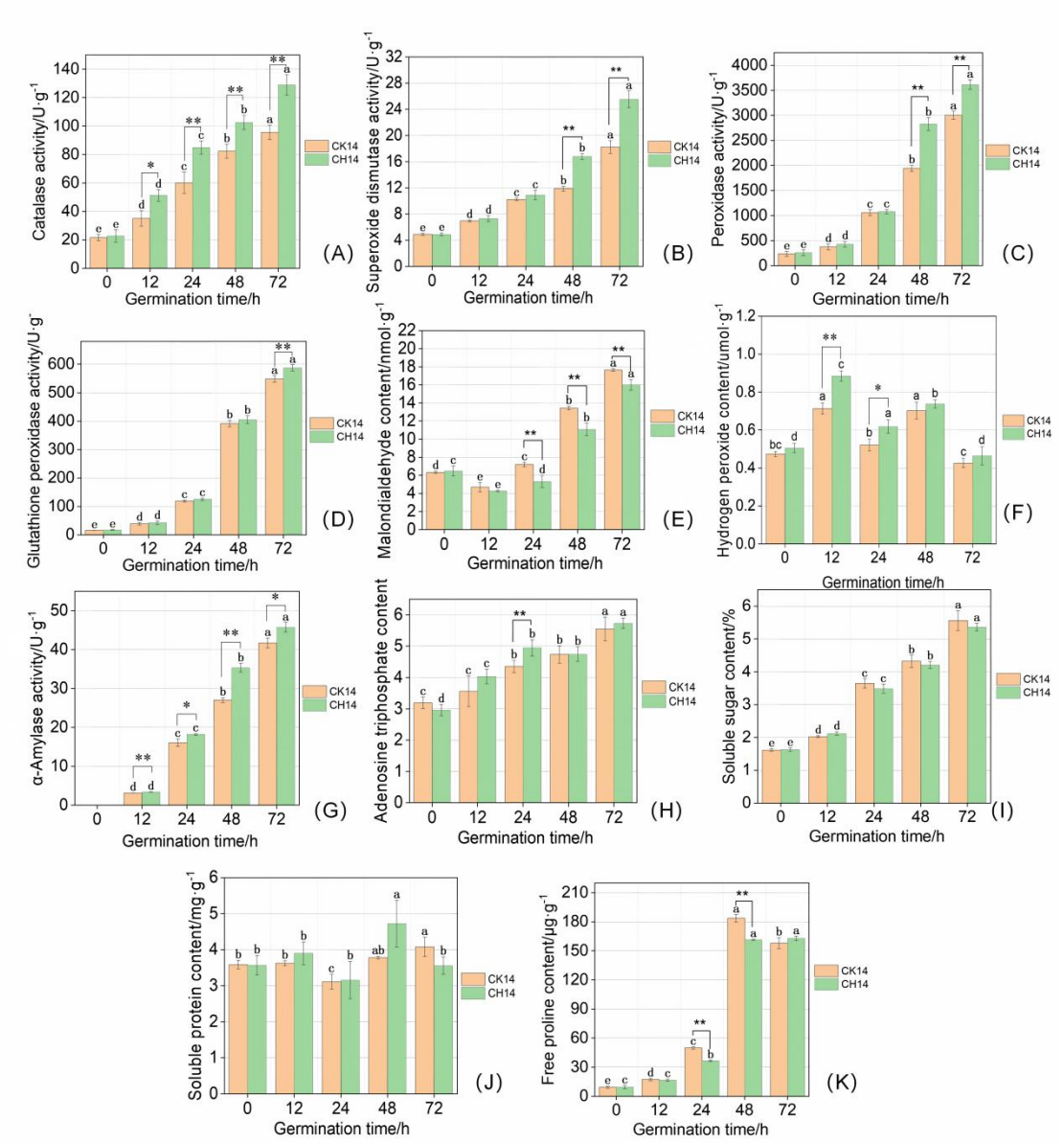

Catalase activity/U·g-1
Germination time/h
CK14
CH14
(A)
Superoxide dismutase activity/U·g-1
(B)
Peroxidase activity/U·g-1
(C)
Glutathione peroxidase activity/U·g-1
(D)
Malondialdehyde content/nmol·g-1
(E)
Hydrogen peroxide content/umol·g-1
(F)
α-Amylase activity/U·g-1
(G)
Adenosine triphosphate content
(H)
Soluble sugar content/%
(I)
Soluble protein content/mg·g-1
(J)
Free proline content/μg·g-1
(K)

Figure 3

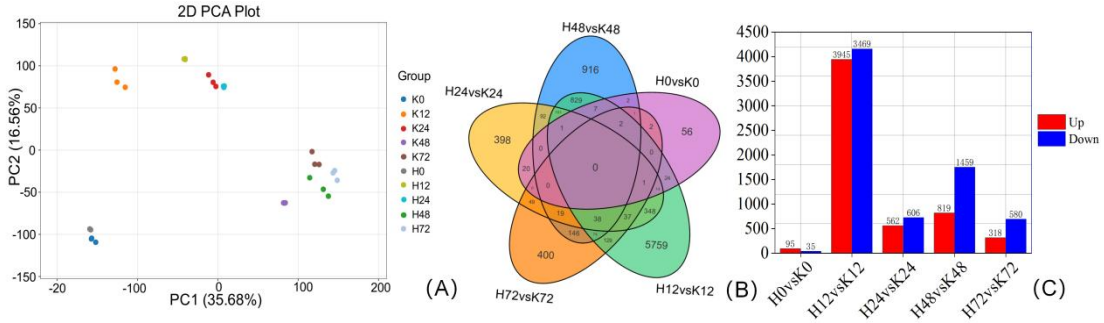

2D PCA Plot
PC2 (16.56%)
PC1 (35.68%)
Group
K0
K12
K24
K48
K72
H0
H12
H24
H48
H72
(A)
H48vsK48
H0vsK0
H24vsK24
H72vsK72
H12vsK12
916
56
398
400
5759
(B)
Up
Down
H0vsK0
H12vsK12
H24vsK24
H48vsK48
H72vsK72
(C)

Figure 4


Tryptophan metabolism
Auxin
auxin influx carrier
transport inhibitor response 1
auxin-responsive protein IAA
auxin response factor
auxin-responsive protein IAA
auxin responsive GH3 gene family
SAUR family protein
Cell enlargement
Plant growth
receptor protein kinase TMK
L-tryptophan---pyruvate aminotransferase
SAUR family protein
Auxin bosynthesis
Abscisic acid response
Zeathn biosynthesis
Cytokinine
cytokinin receptor
histidine-containing phosphotransfer peotein
GARP family transcription factor, ARR-B subfamily
two-component response regulator ARR-A family
Cell division
Shoot initiation
Diterpenoid biosynthesis
Gibberellin
gibberellin receptor GID1
DELLA protein
phytochrome-interacting factor
Stem growth induced germination
Carotenoid biosynthesis
Abscisic acid
abscisic acid receptor PYR/PYL family
protein phosphatase 2C
serine/threonine-protein kinase SRK2
ABA responsive element binding factor
Cell division
Shoot initiation
Cysteine and methionine metabolism
Ethylene
ethylene receptor
serine/threonine-protein kinase CTR1
mitogen-activated protein kinase kinase
ethylene-insensitive protein 2
ethylene-insensitive protein 3
Fruit ripening
Senescence
Brassinosteroid biosynthesis
Brassinosteroid
brassinosteroid insensitive 1-associated receptor kinase 1
protein brassinosteroid insensitive 1
BR-signaling kinase
brassinosteroid resistant 1/2
cyclin D3, plant
Cell division
α-Linolenic acid metabolism
Jasmonic acid
coronatine-insensitive protein 1
jasmonate ZIM domain-containing protein
transcription factor MYC2
Senescence
Stress response
Phenylalanine metabolism
Salicylic acid
regulatory protein NPR1
transcription factor TGA
pathogenesis-related protein 1
Disease resistance
Auxin
Cytokinine
Gibberellin
Abscisic acid
Ethylene
Brassinosteroid
Jasmonic acid
Salicylic acid
Cytokinin
Zscore
-1 0 1 2 3
phytosulfokine
brassinosteroid insensitive 1-associated receptor kinase 1
calmodulin
calcium-dependent protein kinase
calmodulin
glutamine synthetase
indole-3-pyruvate monooxygenase
Plant growth
Tryptophan metabolism
Auxin bosynthesis

Figure 5

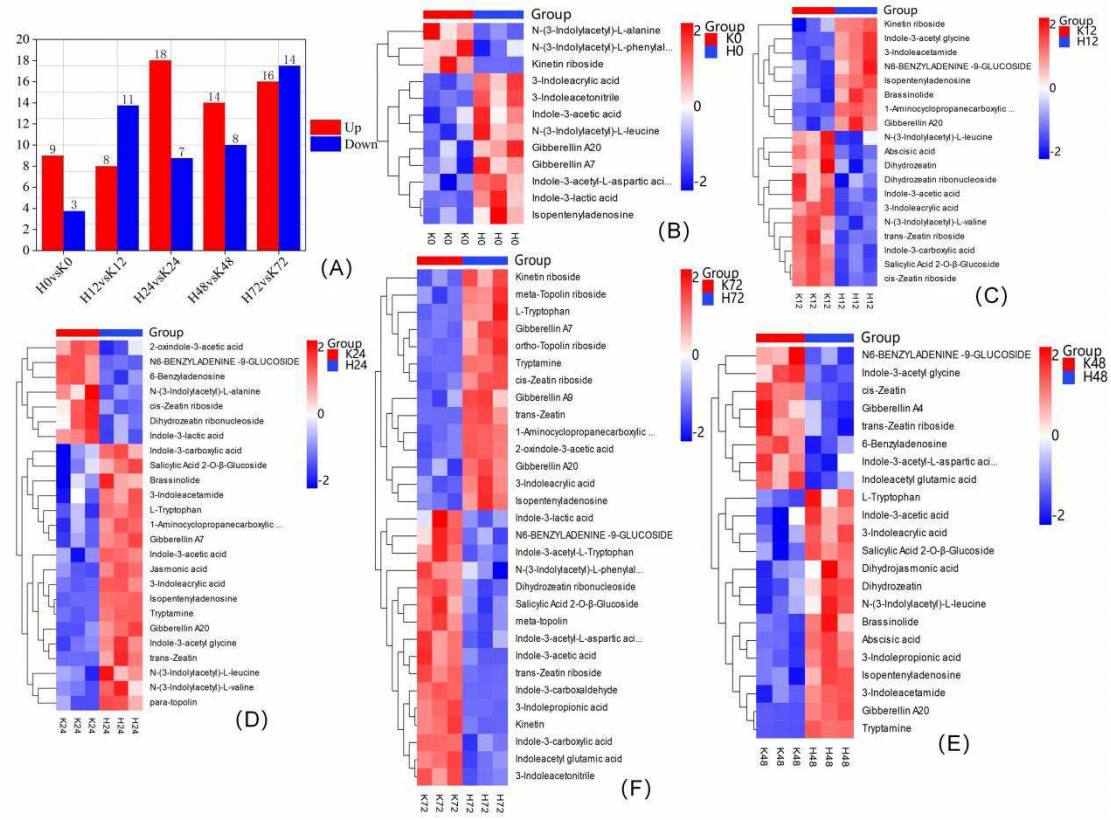

(A)
H0vsK0
H12vsK12
H24vsK24
H48vsK48
H72vsK72
Up
Down
(B)
(C)
(D)
(E)
(F)

Figure 6

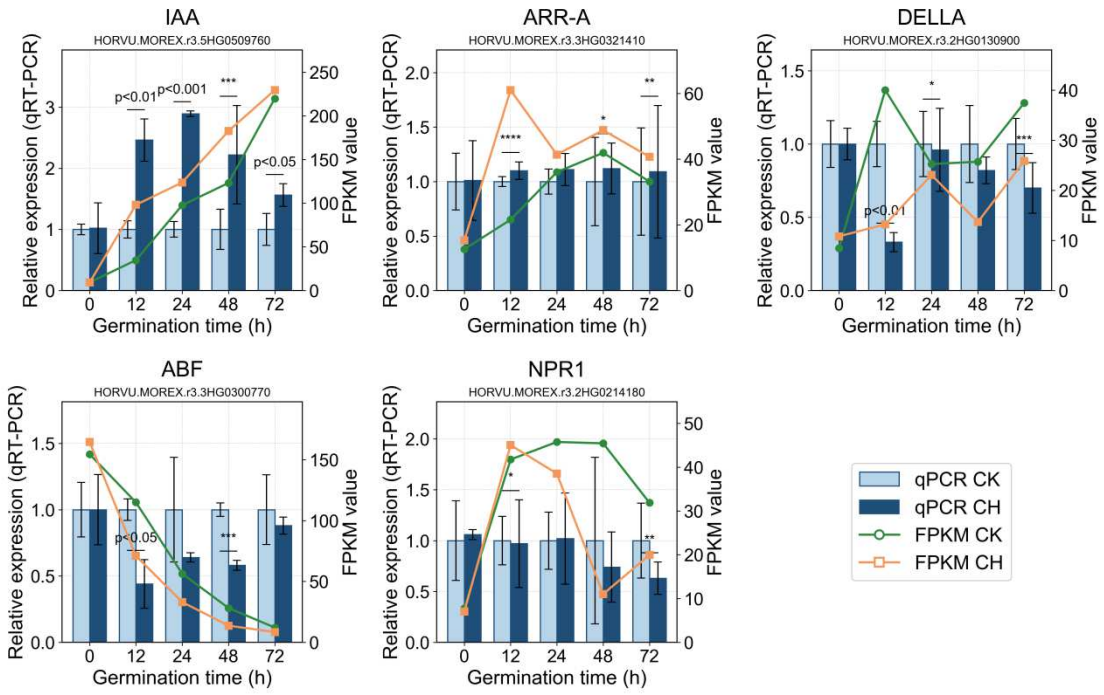

IAA
HORVU.MOREX.r3.5HG0509760
ARR-A
HORVU.MOREX.r3.3HG0321410
DELLA
HORVU.MOREX.r3.2HG0130900
ABF
HORVU.MOREX.r3.3HG0300770
NPR1
HORVU.MOREX.r3.2HG0214180
Relative expression (qRT-PCR)
FPKM value
Germination time (h)
qPCR CK
qPCR CH
FPKM CK
FPKM CH

Figure 7

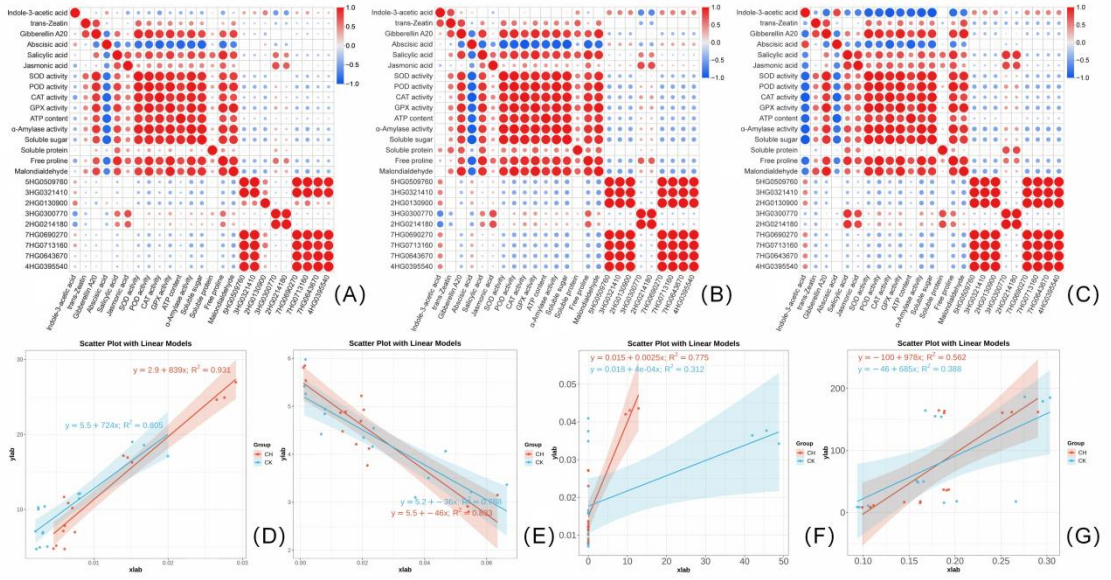


Table 1

Year	Treatment	Emergence peak (plants·m^{-2})	Effective panicles (panicles·m^{-2})	Effective panicles per plant	Grains per spike	1000-grain weight (g)	Grain yield (kg·ha^{-1})
2025	CK	630.67 ± 14.71 b	354.89 ± 11.08 b	1.377 ± 0.050 a	47.04 ± 0.77 a	47.06 ± 0.28 a	6611.10 ± 59.80 b
2025	CH	684.67 ± 11.00 a	382.78 ± 6.87 a	1.447 ± 0.068 a	48.57 ± 0.67 a	46.38 ± 0.31 b	7061.10 ± 137.08 a
2026	CK	648.11 ± 6.71 b	338.56 ± 12.41 b	1.313 ± 0.051 a	46.67 ± 1.18 a	46.89 ± 0.27 a	6262.44 ± 106.75 b
2026	CH	678.11 ± 9.01 a	376.55 ± 9.93 a	1.303 ± 0.058 a	47.95 ± 0.41 a	46.17 ± 0.74 a	6597.44 ± 91.35 a
P_year		0.407	0.094	0.014	0.315	0.481	<0.001
P_treat		<0.001	<0.001	0.391	0.017	0.027	<0.001
P_year ×treat		0.089	0.419	0.261	0.801	0.953	

Note: Values are mean ± SD (n = 3 plots). CK, non-magnetized control; CH, magnetic field treatment. Within each year and indicator, different lowercase letters indicate significant differences between CH and CK based on independent-sample t-tests ($P < 0.05$). P_year, P_treat, and P_year×treat represent the main effect of year, the main

1238 effect of treatment, and the year×treatment interaction, respectively, determined by
1239 two-way ANOVA.

Supplementary Files

This is a list of supplementary files associated with this preprint. Click to download.

- SupplementaryFigure12.pdf
- SupplementaryTable1.docx
- SupplementaryTable2.xlsx
- SupplementaryTable3.xlsx
- SupplementaryTable4.docx